Influence of initial tunneling step on the return energy of high-order harmonic generation

Xu-Zhen Gao [1,2,3] Alexandra S. Landsman [4,*] Huabao Cao [1,3] Yanpeng Zhang,[2] Yishan Wang,[1,3]
Yuxi Fu [1,3,†] and Liang-Wen Pi [1,3,‡]

[1]*State Key Laboratory of Transient Optics and Photonics,*
Xi'an Institute of Optics and Precision Mechanics of the Chinese Academy of Sciences, Xi'an 710119, China
[2]*Key Laboratory for Physical Electronics and Devices of the Ministry of Education & Shaanxi Key Lab of Information Photonic Technique,*
Xi'an JiaoTong University, Xi'an 710049, China
[3]*University of Chinese Academy of Science, Beijing 100049, China*
[4]*Department of Physics, the Ohio State University, Columbus, Ohio 43210, USA*

To investigate high-order harmonic generation in a monochromatic laser field, we derive an analytical expression for the return energy of an electron as a function of the time interval between ionization and return. We then expand the expression for kinetic energy to second order with respect to the Keldysh parameter γ. In this expansion, the zero-order term is the return energy in the simple man model and the second-order term corresponds to corrections to this model. The origin of this additional kinetic energy is frequently attributed to the nonzero exit of the initial tunneling step. Here, we show that this commonly used picture is incomplete. We present a framework to fully understand the additional kinetic energy as resulting from additive contributions of zero-order and second-order velocities. Our results show that the nonzero velocity of the initial tunneling step has a quantifiable effect on the cutoff energy measured in high harmonic generation (HHG). This opens the door to experimentally addressing the question of the initial electron velocity at the tunnel exit, with important implications for the correct calibration of the attoclock, as well as our interpretation of the strong field-ionization process more broadly.

I. INTRODUCTION

Ultrafast science uses experimental observables to answer fundamental questions such as the tunneling time delay, which has been debated since the birth of quantum mechanics [1,2]. Generally, experiments map the initial dynamics of electron motion to observable quantities. Hence, the attoclock measurement maps the tunneling time of the electron to its final momentum distribution [3,4]. Similarly, high harmonic emission maps the dynamics at ionization time to energy at recombination time via the energy of the emitted photons [5–7]. The higher the energy structure observed in the final energy distribution of emitted electrons provides information on electron emission in nanotip-enhanced fields [8–10].

Recently, there have been heated discussions on the importance of nonadiabatic effects near the tunnel exit [11–13] and what it means for the proper description of the electron wavepacket [14]. This also has implications for the tunneling time delay, although a proposal exists [15] to unify both the instantaneous tunneling picture and the Wigner time delay [16] interpretation under the strong field approximation (SFA).

Here, we focus on high-order harmonic radiation, which is produced when a low-frequency strong field interacts with atoms or molecules. The process, known as high harmonic generation (HHG), can produce photon frequencies which are hundreds of times higher than that of incident radiation [17–19]. HHG is typically explained using the simple man three-step model, with the first step corresponding to tunnel ionization [20,21]. In the second step, the electron dynamics are dominated by the strong laser field and can be treated classically. The recombination step of this highly nonlinear process links the tunneling exit and return time by the emitted photon energy, enabling attosecond timescale and nanometer spatial scale resolution in experiments [22,23].

Although the simple man model has proven very fruitful in interpreting HHG, it was previously shown that there is a distinct deviation of ionization time between this model and the experimentally reconstructed ionization time [5]. To explain this, we use perturbation methods to analyze the electron dynamics involved in HHG to quantize the additional kinetic energy gained by the recombining electron beyond the predictions of the simple man model. The harmonic dipole under SFA is calculated using the saddle-point approximation (SPA), where the integral is changed into a series of discrete distributions from the saddle points of the integrand [24–27]. This quantum orbit theory, based on the Lewenstein model, plays an important role in understanding the underlying electron dynamics [28–35]. In particular, the ionization time of saddle points agrees well with the reconstructed ionization time [5]. At the same time, the quantum trajectory method connects to the simple man model via the classical action in the exponent, corresponding to propagation in the laser field [5,33].

---

*landsman.7@osu.edu
†fuyuxi@opt.ac.cn
‡lwpi@opt.ac.cn

Note that our analysis focuses on the return electron energy, which will determine the frequency of the emitted radiation. However, the conversion efficiency and coherence properties of the emitted harmonics will depend on the phase of the induced atomic dipole moment. This phase is related to the action acquired by the electron during its motion in the laser field, with its value affected by the quantum effects of tunneling, diffusion, and interference [36]. A discussion of this, as well as a detailed investigation of the transition dipole moment and its impact on recollision trajectories can be found in a recent publication [37].

From saddle-point equations, it is known that the times (including ionization time and return time) and dynamics are all complex valued. Using the Keldysh parameter $\gamma = \sqrt{I_p/(2U_p)}$ as a perturbation term, we expand the return energy to second order. We then show that the difference between the return energy in the Lewenstein model and the classical energy in the simple man model corresponds to the additional kinetic energy contained in the second order of this expansion.

The cutoff law, corresponding to the highest possible emitted harmonic frequency, is $E_c = 3.17U_p + I_p$ [20] in the simple man model and $E_c = 3.17U_p + 1.32I_p$ [24] in the quantum Lewenstein model. Previously, the $0.32I_p$ difference between these two models was explained by the initial position of the tunneled electron [5]. In particular, it is typically believed that this additional kinetic energy is acquired as the electron moves from the initial tunneled position to the origin during the recombination process [24,38,39]. In this paper, we provide insight into the origin of the energy upshift in emitted harmonics, showing that the nonzero position of the tunneled electron only partially explains this additional energy of $0.32I_p$, and that a nonzero initial velocity is also necessary to more accurately account for the difference between the simple man and Lewenstein models.

To this end, we use perturbation methods to calculate the higher-order velocities both in the tunneling and propagation steps, showing that the additional kinetic energy can be explained as resulting from additive contributions of tunneling and classical velocities. We also show how nonadiabatic effects during tunneling affect both the tunneling velocity and the electron velocity in the continuum. Hence including velocity at the tunnel exit is necessary to fully explain the dynamics underlying HHG.

The rest of the paper is organized as follows. In Sec. II, we briefly describe the saddle-point equations, which are then used to derive the return energy to the first two orders. We then show that the second-order expansion corresponds to the additional kinetic energy of returning electrons. We also expand the electron tunneling velocity and the return velocity up to second order. We demonstrate how the additional kinetic energy results from the interference of zero- and second-order velocities. We summarize our results and present conclusions in Sec. III.

II. THEORY AND DISCUSSION

A. Analytical expression of return energy in HHG

The saddle-point method, which allows the analytical evaluation of highly oscillating functions, is used to calculate the

HHG dipole under the strong field approximation. The saddle points are located at positions where the phase of integrand having zero derivative with respect to all integral variables, i.e., tunneling time t_i, return time t_r, and canonical momentum p_{st}. The saddle-point equations are given by

$$\nabla_{p_{st}} S(p_{st}, t_r, \tau) = x(t_r) - x(t_r - \tau) = 0, \tag{1}$$

$$\frac{\partial S(p_{st}, t_r, \tau)}{\partial \tau} = \frac{[p_{st} - A(t_r - \tau)]^2}{2} + I_p = 0, \tag{2}$$

$$\frac{\partial S(p_{st}, t_r, \tau)}{\partial t_r} = \frac{[p_{st} - A(t_r)]^2}{2} - \frac{[p_{st} - A(t_r - \tau)]^2}{2} = \hbar\omega_q, \tag{3}$$

where

$$S = \int_{t_r-\tau}^{t_r} \left(\frac{[p_{st} - A(t'')]^2}{2} + I_p \right) dt'' \tag{4}$$

is the semi-classical action and it represents the phase factor acquired during the propagation process. t_r is the electron return time and $\tau = t_r - t_i$ represents the time interval between ionization and return

$$x(t) = \int_{-\infty}^{t} \left(\frac{[p_{st} - A(t'')]}{2} \right) dt'' \tag{5}$$

is the displacement during the propagation process, and ω_q is the frequency of the qth-order harmonic radiation. Note that the time is normalized to be periodic in 2π, thereby corresponding to the phase of the laser field.

Throughout the paper a monochromatic laser field is used, given by $A(t) \equiv -A_0 \sin(t)$, where A_0 is the amplitude of the vector potential. Equation (1) can be written in the form of

$$\int_{t_r-\tau}^{t_r} \left(\frac{[p_{st} - A(t'')]}{2} \right) dt'' = 0. \tag{6}$$

The canonical momentum is then given by

$$p_{st} = \frac{A_0[\cos(t_r) - \cos(t_r - \tau)]}{\tau}. \tag{7}$$

Inserting this expression into Eq. (2) and using trigonometric functions, we obtain

$$\sin\left(t_r - \frac{\tau}{2}\right) a(\tau) - \cos\left(t_r - \frac{\tau}{2}\right) s(\tau) = i\gamma, \tag{8}$$

where

$$a(\tau) = \cos\left(\frac{\tau}{2}\right) - \frac{2\sin\left(\frac{\tau}{2}\right)}{\tau}, \tag{9}$$

$$s(\tau) = \sin\left(\frac{\tau}{2}\right), \tag{10}$$

where $\gamma \equiv \sqrt{I_p/2U_p}$ is the Keldysh parameter and $U_p \equiv A_0^2/4$ represents the ponderomotive energy in the laser field.

Using trigonometric identities, $\sin(t_r - \tau/2)$ and $\cos(t_r - \tau/2)$ can be expressed in the form of $a(\tau)$ and $s(\tau)$, see Eqs. (A1) and (A2) in the Appendix. Similarly, the electron kinetic energy at return time, which is a function of t_r and τ, can be expressed as a function of $a(\tau)$

and $s(\tau)$

$$E_{\mathrm{re}} = \frac{[p_{\mathrm{st}} - A(t_r)]^2}{2}$$

$$= \frac{A_0^2}{2} \left[a \frac{ia\gamma + (s\sqrt{a^2 + s^2 + \gamma^2})}{a^2 + s^2} \right]^2$$

$$+ \frac{A_0^2}{2} \left[s \frac{-is\gamma + (a\sqrt{a^2 + s^2 + \gamma^2})}{a^2 + s^2} \right]^2, \quad (11)$$

where we set $a \equiv a(\tau)$ and $s \equiv s(\tau)$. This expression corresponds to Eq. (37) in Ref. [24]. However, the ionization equation, or Eq. (2), requires that the times and canonical momentum in the saddle-point equations are all complex valued, which has important implications for our key findings.

Following the authors of Ref. [24], τ can be expressed as a sum of real and imaginary parts. The real part of the time interval τ_0 has the meaning of propagation time, while the imaginary part can be viewed as higher-order perturbation terms. One can express the time interval as $\tau = \tau_0 + i\gamma\tau_1 + i\gamma^2\tau_2$, in which the Keldysh parameter γ is small. Note that the static field limit $\gamma \to 0$ corresponds to fully adiabatic tunneling.

We are now in a position to obtain the Taylor expansion, with respect to γ, for the electron return energy. We find that the first-order expansion is an imaginary value and takes the form

$$E_{\mathrm{re}}^{(1)} = i\gamma \frac{8a_0 s_0 (a_0^2 - s_0^2)}{\tau_0 (a_0^2 + s_0^2)^2}$$

$$\times \left[2a_0 s_0 \tau_1 + \tau_0 (\sqrt{a_0^2 + s_0^2} + a_0^2 \tau_1 + s_0^2 \tau_1) \right], \quad (12)$$

where we set $a_0 \equiv a(\tau_0)$ and $s_0 \equiv s(\tau_0)$. However, the imaginary part should be zero considering that the return energy is an observable quantity. The expression for τ_1 can be obtained from this constraint

$$\tau_1 = -\frac{\tau_0 \sqrt{a_0^2 + s_0^2}}{2a_0 s_0 + \tau_0 (a_0^2 + s_0^2)}. \quad (13)$$

The second-order expression has both imaginary and real parts. For the same reason, the imaginary part is required to be zero, leading to

$$\mathrm{Im}\left(E_{\mathrm{re}}^{(2)}\right) = \frac{8a_0 s_0 (a_0^2 - s_0^2)(2a_0 s_0 + a_0^2 \tau_0 + s_0^2 \tau_0)}{\tau_0 (a_0^2 + s_0^2)^2} \tau_2$$

$$= 0. \quad (14)$$

It is obvious that the terms in the numerator only equal to zero at particular values of τ_0. Therefore, $\tau_2 = 0$ is obtained from this constraint. Plugging τ_1 and τ_2 in E_{re} and simplifying the expression further, we obtain a more physically relevant expression for the return energy

$$E_{\mathrm{re}} = \frac{A_0^2}{4} \frac{8a_0^2 s_0^2}{a_0^2 + s_0^2} - \frac{A_0^2}{4} \frac{16[a_0^2 s_0^3 (s_0 + a_0\tau_0)]\gamma^2}{(a_0^2 + s_0^2)(2a_0 s_0 + a_0^2 \tau_0 + s_0^2 \tau_0)^2}$$
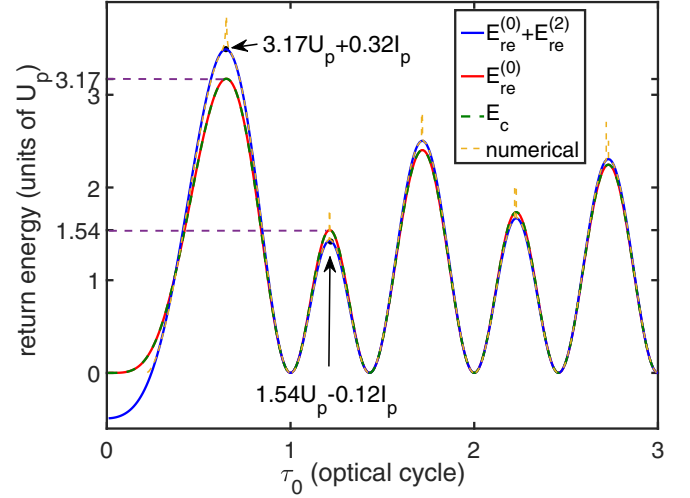
$$+ O(\gamma^3). \quad (15)$$

FIG. 1. The comparison of zero-order return energy, given in Eq. (16) (red solid line), and the return energy predicted within the simple man model (green dashed line). The two lines coincide exactly. The blue solid line shows the sum of the first two orders of return energy as a function of τ_0, given by Eq. (15). The orange line is the numerical solution of saddle-point equations. Note that $\gamma = 0.7$ is used in the calculation. The cutoff energy of the first two returns are marked by the two black dots: the first dot shows larger than classical return energy while the second shows smaller than classical kinetic energy. The difference between the blue line and the red line is the second-order return energy in the Lewenstein model. The propagation time is in units of optical cycle and the return energy is expressed in units of U_p.

Let us denote

$$f(\tau_0) = \frac{8a_0^2 s_0^2}{a_0^2 + s_0^2}, \quad (16)$$

$$g(\tau_0) = -\frac{8[a_0^2 s_0^3 (s_0 + a_0\tau_0)]}{(a_0^2 + s_0^2)(2a_0 s_0 + a_0^2 \tau_0 + s_0^2 \tau_0)^2}, \quad (17)$$

then Eq. (15) can be divided into two parts: the zero-order and second-order expansions

$$E_{\mathrm{re}}^{(0)} = f(\tau_0)U_p, \quad (18)$$

$$E_{\mathrm{re}}^{(2)} = 2g(\tau_0)\gamma^2 U_p = g(\tau_0)I_p. \quad (19)$$

The zero-order expression $E_{\mathrm{re}}^{(0)}$, shown in Fig. 1, represents the energy gained in the laser field. We prove that it is exactly the same expression as the return energy in the simple man model (see Appendix B)

$$E_{\mathrm{re}}^{(0)} = 2U_p[\sin(t_r) - \sin(t_r - \tau_0)]^2 = E_c. \quad (20)$$

The same expression of the return energy is shown in Eq. (6.198) of Ref. [40]. This can also be observed in Fig. 1, where the curves $E_{\mathrm{re}}^{(0)}$ and E_c coincide exactly.

The numerical solution of the saddle-point equations is shown in Fig. 1 as an orange line. There are spikes near the cutoff energy at each return, which are singularities due to the second-order expansion used in the saddle-point method and can be fixed by the uniform approximation [41]. It is clearly shown that our second-order analytical expression of
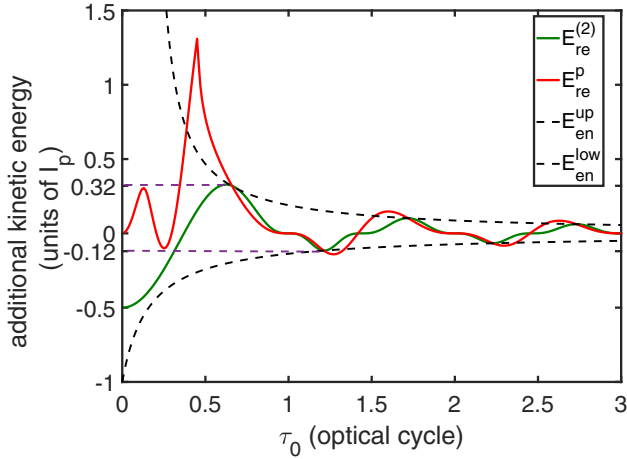
FIG. 2. The second-order return energy expressed in units of I_p (green solid line). The cutoff energy of first two returns are marked by dashed horizontal lines. The black dashed curves show the asymptotic behavior of the second-order energy. The upper envelope curve corresponds to first set of extreme curve $E_{en}^{up} = 1/(\tau_0 - 1)$, and it represents the cutoff energy of odd returns. The lower envelope curve corresponds to second set of extreme curve $E_{en}^{low} = 1/(-\tau_0 - 1)$, and represents even returns. The red line is the additional kinetic energy, given by Eq. (24), which assumes zero initial velocity, but nonzero initial displacement due to tunneling. This comparison shows that the zero initial velocity assumption might not accurately account for the return energy.

the return energy (blue line) has excellent agreement with the numerical solution, which confirms the validity of our derivation. There remains a difference between the final expression of return energy and return energy in the simple man model. The difference is the second-order return energy we derived, which is the key result of this paper. This closed-form analytical expression for return energy, which can be divided into zero-order and second-order expressions with respect to γ, allows for a systematic study of the nonadiabatic effects.

The second-order term $E_{re}^{(2)}$ is shown in Fig. 2, in units of I_p. The curve oscillates around 0 and shows positive values in odd returns and negative values in even returns. The amplitude decays with propagation time τ_0, eventually decaying to zero. This suggests that the additional kinetic energy is caused by the quantum nature of the ionization process and can be omitted for very long trajectories, as the quantum effects fade away and only the electron's classical motion remains.

The cutoff energy is the maximum possible energy of the returning electron and corresponds to the maximum of $E_{re}^{(0)}$. This can be obtained by solving the following equation:

$$\frac{dE_{re}^{(0)}}{d\tau_0} = \frac{16 a_0 s_0}{\left(a_0^2 + s_0^2\right)^2} U_p$$
$$\times \left[(a_0 - s_0)(a_0 + s_0)\left(\frac{1}{2}a_0^2 + \frac{1}{2}s_0^2 + \frac{1}{\tau_0}a_0 s_0\right)\right]. \tag{21}$$

There exist two sets of solutions: one is $a_0 = -s_0$ and the other is $a_0 = s_0$. Plugging these two sets of solutions into

Eq. (19), one can obtain two types of envelope curves (black dashed lines in Fig. 2).

The first set of second-order return energy corresponds to

$$E_{en}^{up} = \frac{1}{\tau_0 - 1}. \tag{22}$$

The odd return cutoff energy situates on this curve. The second set of second-order return energy corresponds to

$$E_{en}^{low} = \frac{1}{-\tau_0 - 1}. \tag{23}$$

The cutoff energy of the even returns situate on this curve.

In the past, the origin of additional kinetic energy was commonly attributed to the nonzero initial position of the tunneled electron. In particular, the tunneled electron has an approximate initial position $x_0 = -I_p/E_0$, where E_0 is the amplitude of the electric field. Hence the electron returns to the origin when $x(t_f) - x(t_i) + x_0 = 0$ is satisfied. This equation is solved numerically, with additional kinetic energy given by

$$E_{re}^{p} = \frac{1}{2}v_f^2 - E_c, \tag{24}$$

which is shown in the red solid line in Fig. 2. The expression of the return energy second-order expansion $E_{re}^{(2)}$ is shown in the green solid line. Although the two curves have intersection points at each return, the intersection points are not the cutoff energy except for the first return. In the following section, we will explore the physical explanation for the additional kinetic energy by solving the electron velocity up to second-order using perturbative expansion. The above-described result will also be compared to our findings.

B. Higher-order expression for velocities of tunneling and classical propagation steps

In the preceding discussion, a common assumption was made of zero electron velocity at the tunnel exit. This assumption neglected the influence of nonadiabatic effects. Under nonadiabatic conditions, it is more accurate to take into account the initial electron velocity. To calculate the final velocity, we need to solve the tunneling time and return time of the saddle points. The return time is expressed as $t_r = t_r^{(0)} + i\gamma t_r^{(1)} + \gamma^2 t_r^{(2)}$. In Appendix A, we derive each term of this expression by the expansion of $\sin(t_r - \tau/2)$ and $\cos(t_r - \tau/2)$ expressed by Eqs. (A1) and (A2)

$$t_r^{(0)} = \arctan\left(\frac{s_0}{a_0}\right) + \frac{\tau_0}{2} + T\left\lfloor\left[\frac{\tau_0}{2 * 2\pi} + \frac{1}{2}\right]\right\rfloor, \tag{25}$$

$$t_r^{(1)} = 0, \tag{26}$$

$$t_r^{(2)} = \frac{\tau_0 \cos(\tau_0) - \sin(\tau_0)}{2[\tau_0 - \sin(\tau_0)]^2}. \tag{27}$$

The bracket $\lfloor \rfloor$ of the last term in Eq. (25) means round down to an integer. Therefore, the return time can be expressed as $t_r = t_r^{(0)} + \gamma^2 t_r^{(2)}$. Also the initial time, which is expressed by $t_i = t_i^{(0)} + i\gamma t_i^{(1)} + \gamma^2 t_i^{(2)}$, can be obtained

$$t_i^{(0)} = t_r^{(0)} - \tau_0, \tag{28}$$

$$t_i^{(1)} = t_r^{(1)} - \tau_1 = -\tau_1, \tag{29}$$

$$t_i^{(2)} = t_r^{(2)} - \tau_2 = t_r^{(2)}. \tag{30}$$

The motion of the electron can be described as follows: first, it proceeds in imaginary time with an imaginary velocity in the tunneling process, then it propagates in real time with real velocity, corresponding to propagation time, and finally it recombines with the parent ion.

In the following derivation, we solve for the velocity at tunneling exit and return time. The canonical and vector potentials are expressed in units of A_0. One can express the expansion as $p_{st} = p_{st}^{(0)} + i\gamma p_{st}^{(1)} + \gamma^2 p_{st}^{(2)}$, then each order of this expression can be derived from Eq. (7). Plugging τ and t_r into Eq. (7) and expanding the left-hand side to second order, then simplifying the expansion further by trigonometric functions one can obtain each-order of canonical momentum as follows (Appendix C explains why $p_{st}^{(1)} = 0$):

$$p_{st}^{(0)} = -\sin\left(t_i^{(0,)}\right) \tag{31}$$

$$p_{st}^{(1)} = 0, \tag{32}$$

$$p_{st}^{(2)} = -\frac{\sqrt{a_0^2 + s_0^2}}{2\left[2a_0^2 s_0^2 + \tau_0\left(a_0^2 + s_0^2\right)\right]}. \tag{33}$$

The electron velocity at the tunnel exit is

$$v_i = p_{st} - A[\mathrm{Re}(t_i)] = p_{st} - A\left(t_i^{(0)} + \gamma^2 t_i^{(2)}\right). \tag{34}$$

Plugging $t_i^{(0)}$ and $t_i^{(2)}$ in this expression and expanding it to second order, while using $v_i^{(0)} = 0$, the electron velocity at the tunneling exit is given by

$$v_i \simeq v_i^{(2)} \gamma^2 = \left[p_{st}^{(2)} + t_i^{(2)} \cos\left(t_i^{(0)}\right)\right]\gamma^2. \tag{35}$$

The electron velocity at return time is

$$v_{re} = p_{st} - A[\mathrm{Re}(t_r)] = p_{st} - A\left(t_r^{(0)} + \gamma^2 t_r^{(2)}\right). \tag{36}$$

Plugging $t_r^{(0)}$ and $t_r^{(2)}$ in this expression and expanding it to second order, v_{re} can be expressed as

$$v_{re} \simeq \left[-\sin\left(t_i^{(0)}\right) + \sin\left(t_r^{(0)}\right)\right]$$
$$+ \left[p_{st}^{(2)} + t_r^{(2)}\cos\left(t_r^{(0)}\right)\right]\gamma^2. \tag{37}$$

The classical velocity, which we define as the velocity gained in the second step, is the difference value of the tunneling velocity and return velocity. It contains zero-order and second-order terms $v_c \simeq v_c^{(0)} + \gamma^2 v_c^{(2)}$, taking the form

$$v_c^{(0)} = -\sin\left(t_i^{(0)}\right) + \sin\left(t_r^{(0)}\right), \tag{38}$$

$$v_c^{(2)} = t_r^{(2)}\left[\cos\left(t_r^{(0)}\right) - \cos\left(t_1^{(0)}\right)\right]. \tag{39}$$

Now, the return velocity is the sum of the zero-order and second-order perturbation terms

$$v_{re} = v_c^{(0)} + \gamma^2 v_i^{(2)} + \gamma^2 v_c^{(2)}. \tag{40}$$

The zero order and second order of v_{re} are shown in Fig. 3. The zero-order return velocity $v_c^{(0)}$ is exactly the same as the classical velocity Eq. (20) in the simple man model. The second-order velocity $v_i^{(2)}$ reflects the quantum effect of tunneling and is consistent with the energy gained during nonadiabatic tunneling. The quantum tunneling process not only affects the velocity at the tunneling exit, but also the velocity of the following classical propagation. The two
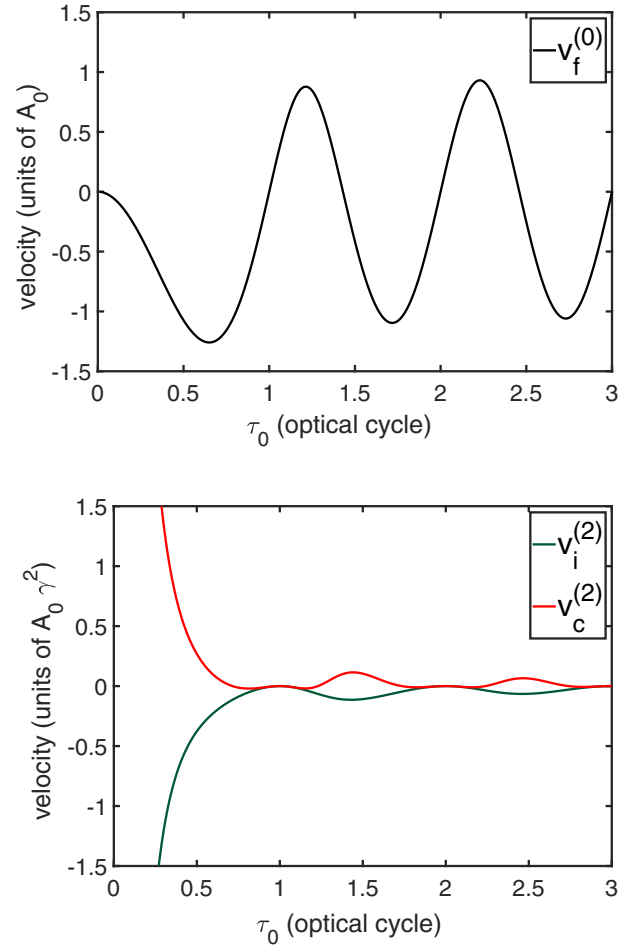

FIG. 3. Upper: Electron return velocity to zero order, corresponding to classical return velocity in the simple man model. Bottom: The second-order correction to return velocity. The red line shows the velocity at the tunneling exit and the green shows the second-order classical velocity. The lines diverge to infinity as $\tau_0 \to 0$ due to the breakdown of perturbation theory.

second-order velocities, v_i^2 and $v_c^{(2)}$, are therefore both responsible for the additional kinetic energy. In the bottom panel of Fig. 3, one can see that the two curves are not convergent when τ_0 tends to zero due to the breakdown of the condition $\tau_0 > \gamma \tau_1$, used for the perturbative expansion.

C. Decomposition of additional kinetic energy and velocity at tunnel exit

Figure 4 illustrates the difference between neglecting the initial velocity and only taking account of position and taking account of both the initial velocity and position, labeled as "Position scenario" and "Velocity scenario," respectively. In the left panel of Fig. 4, the electron appears at the tunnel exit with zero velocity, then it gains classical velocity v_c when returning to the tunneling exit, and finally it acquires additional kinetic energy when returning back to the origin. In this scenario, the nonadiabaticity of the tunneling process is neglected. The right panel of Fig. 4 shows the "Velocity scenario." First, the electron has the second-order velocity $\gamma^2 v_i^{(2)}$ at the tunneling exit, then it gains classical velocity
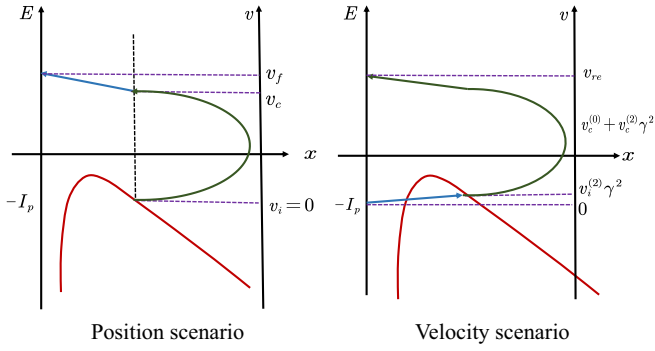
FIG. 4. A sketch of two kinds of scenarios. The vertical axis on the right in the subgraphs shows the velocity at each stage of the three-step model. The left panel describes the position scenario: the electron appears at the tunneling exit with zero velocity, acquires classical energy when returning to the tunneling exit, and acquires additional kinetic energy when returning to the origin. The right panel describes the velocity scenario: The electron has initial velocity $\gamma^2 v_i^{(2)}$ when the propagation process begins and acquires classical velocity $v_c^{(0)} + \gamma^2 v_c^{(2)}$ after returning to the origin.

$v_c^{(0)} + \gamma^2 v_c^{(2)}$ when returning to the origin. In this scenario, the nonadiabatic tunneling process affects both the tunneling exit velocity and classical velocity.

The "Position scenario" is often used to explain the origin of additional kinetic energy. However, it is not consistent with the saddle-point equation, Eq. (1), in which the electron returns to the origin at recombination time. This scenario also leaves out the consideration of nonadiabatic affects during tunneling. What's more, the result cannot suit the second-order analytical expression well. In contrast, the "Velocity scenario" is a rigorous derivation under the second-order perturbation of the saddle-point equations and includes nonadiabatic contributions. The additional kinetic energy obtained in this scenario is calculated and compared with the analytical expression and position result in the following context.

From the calculated return velocity, one can easily obtain the kinetic energy at return time

$$E_{\text{re}} = \tfrac{1}{2} v_{\text{re}}^2 = \tfrac{1}{2} A_0^2 \big(v_c^{(0)} \big)^2 + 2 v_c^{(0)} \big(v_i^{(2)} + v_c^{(2)} \big) I_p. \quad (41)$$

The zero-order kinetic energy is the same as in the simple man model, corresponding to Eq. (20). The second order of kinetic energy is the additional kinetic energy obtained by considering nonadiabatic contributions to velocity, which are not included in the simple man model. The upper panel of Fig. 5 compares the additional kinetic energy obtained when the nonadiabatic contributions to velocity are included (described as the "Velocity scenario" in Fig. 4) with the analytical expression in Eq. (19). The two results show excellent agreement, suggesting that the second-order additional kinetic energy is caused by additive contributions of zero-order and second-order velocities. The two second-order velocities are all induced by the nonadiabatic tunneling process, showing how the tunneling step impacts the return energy. In addition, this can also explain why the additional kinetic energy is in units of I_p.

Note that the second-order kinetic energy is made up of two components: (i) the term resulting from the addition of
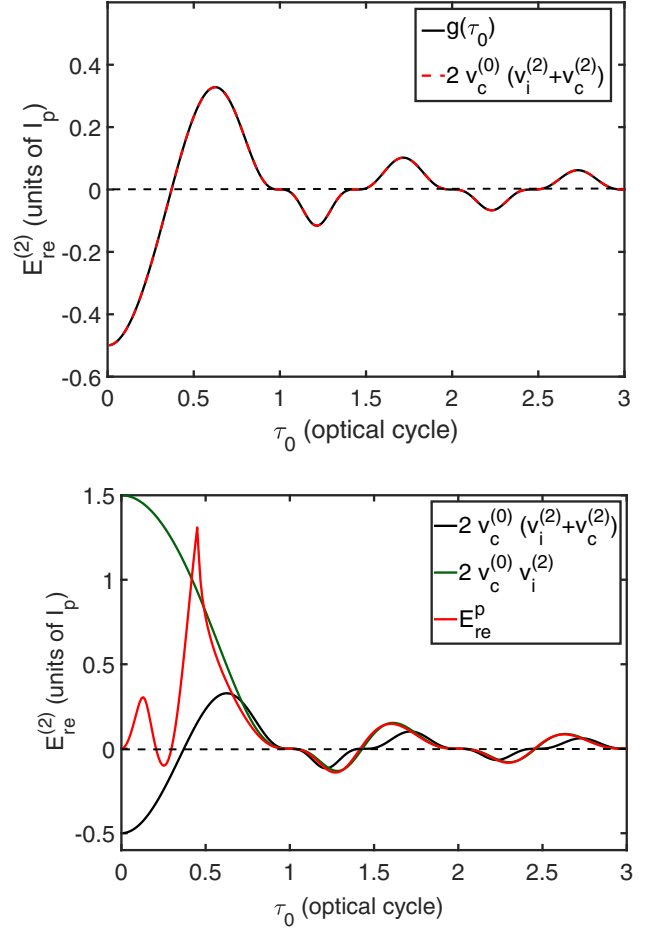

FIG. 5. Upper: The second-order return energy (black solid line) and the additional kinetic energy obtained by using nonzero initial velocity (red dashed line). This scenario shows an excellent agreement with Eq. (19). Bottom: The interference term of second-order tunneling velocity and zero-order classical velocity (green solid line). The additional kinetic energy obtained by assuming zero initial velocity, but nonzero position, corresponding to tunnel exit (red solid line). The good agreement between red and green curves later in the optical cycle means that nonzero initial displacement partially explain the origin of additional kinetic energy.

the zero-order and the second-order tunneling exit velocities and (ii) the second-order classical velocity. Figure 5 compares these two components separately with the adiabatic tunneling prediction, shown in the left panel of Fig. 4. The later figure shows good agreement with the first component, corresponding to (i) above, indicating why the zero velocity at tunnel exit assumption can partly account for the additional kinetic energy. Considering this good agreement, we further investigate the displacement at the tunneling exit using a perturbative expansion, which can be calculated as

$$x_i = \int_{t_i}^{\text{Re}(t_i)} \left(\frac{[p_{\text{st}} - A(t'')]}{2} \right) dt'', \quad (42)$$

where t_i and p_{st} are the saddle points of ionization time and the canonical momentum, respectively. Within the saddle-point method, the ionized electron tunnels through the barrier on
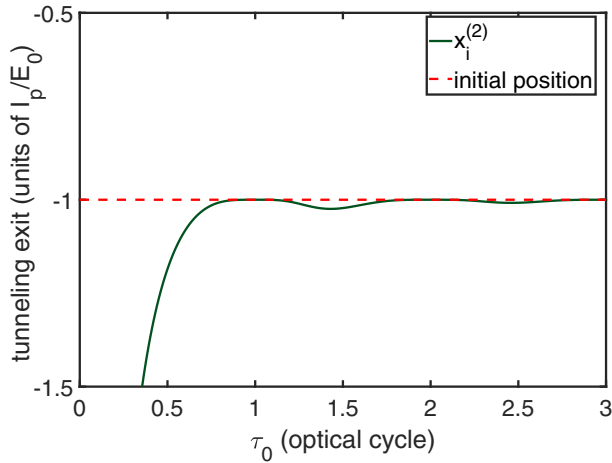
FIG. 6. The comparison of displacement at the tunneling exit in the velocity scenario (green solid line) and the position scenario (red solid line), where the two scenarios are depicted in Fig. 4. The displacement is in units of I_p/E_0, where E_0 is the amplitude of laser field. The two lines only shows very small difference at the cutoff of first and second returns. x_i shows nonconvergence for very small τ_0 due to the breakdown of perturbation theory.

the complex time plane, moving from origin at time t_i to the tunneling exit at time $\text{Re}(t_i)$. Plugging the expressions for t_i [Eqs. (28) to (30)] and p_{st} [Eqs. (31) and (32)] to the equation above, one can find the zero-order $x_i^{(0)}$ and first-order $x_i^{(1)}$ terms to be zero and the second-order term $x_i^{(2)}$ takes the form

$$x_i = \gamma^2 x_i^{(2)} = \tfrac{1}{2}\gamma^2 \left(t_i^{(1)}\right)^2 \cos\left(t_i^{(0)}\right). \tag{43}$$

The result is shown as a green solid line in Fig. 6, where the displacement is in units of I_p/E_0. It is clear that the second-order displacement is irrelevant to the second-order expansion of time and velocity. The second-order displacement also has only a minor influence on the cutoff of the first return, as well as the second return cutoff. This helps explain the agreement between the green and red curves, shown in the bottom panel of Fig. 6. Note that the second-order displacement diverges at small τ_0 due to the breakdown of perturbation theory.

The initial conditions after tunneling were extensively debated in recent years. The tunneling process occurs in a time-dependent field, introducing ambiguities in the choice of tunneling coordinates. The perturbative approach presented here gives consistent tunneling exit characteristics with nonadiabatic effects fully included [11–13]. Here, we demonstrated that a second-order expansion in velocity gives a fuller description of the ionization dynamics, more accurately accounting for the additional kinetic energy observed at recombination.

III. CONCLUSION

In conclusion, we investigate the return energy involved in high harmonic generation under strong field approximation using perturbation theory. An analytical expression of return energy, a function of time interval τ, is derived from the saddle-point approximation equations. The saddle-point equation represents the energy conservation law and requires that the time interval is a complex value, with a small γ-dependant imaginary part. The analytical expression is expanded to second-order with respect to γ. The zero-order term of the expansion corresponds to the classical energy gained in a simple man model and the second-order term corresponds to additional kinetic energy.

Although the additional kinetic energy beyond the simple man model is typically explained by the initial electron displacement following tunneling, we show with a more detailed analytical treatment that the tunneling step introduces a nonzero additional velocity both at the tunnel exit and during propagation in the continuum. In particular, we expand the return velocity to several orders within perturbation theory, using the Keldysh parameter γ. The zero-order velocity corresponds to the classical velocity in the simple man model, while the second-order velocities contain the tunneling exit velocity and the correction to the classical velocity. Both second-order contributions are due to the nonadiabatic effects during quantum tunneling. These additional second-order velocities correspond to additional terms in our perturbative expansion, whereas the zero-order velocity corresponds to the classical velocity in the simple man model.

Finally, we calculate a correction to the return energy using a perturbative expansion in velocity. While, as mentioned above, the zero-order return energy is the classical energy in the simple man model, the second order involves the addition of zero-order and second-order velocities (including second-order tunneling exit velocity and second-order classical velocity). We analyze the relative contributions of the different second-order terms, finding that one of them can be accounted for by the initial electron displacement during tunneling (a typical explanation of the additional kinetic energy at return relative to the simple man model). However, the other term in the second-order expansion, resulting from the addition of the zero-order and second-order classical velocities, relies on the nonzero velocity at the tunnel exit and therefore cannot be explained by the initial electron displacement from the parent atom. This establishes a way to experimentally verify the existence of nonzero velocity at the tunnel exit (in the direction of tunneling) by measuring the HHG cutoffs. The definitive experimental answer to this question promises to have profound implications to how we interpret attoclock measurements of tunneling time, which rely on having accurate initial conditions at the tunnel exit.

APPENDIX A: DERIVATION OF RETURN TIME

We use the quadratic sum of trigonometric function in Eq. (8), where $\sin(t_r - \tau/2)$ and $\cos(t_r - \tau/2)$ can be expressed as

$$\sin\left(t_r - \frac{\tau}{2}\right) = \frac{i\sqrt{\frac{I_p}{2U_p}}a(\tau) + s(\tau)\sqrt{a^2(\tau) + s^2(\tau) + \frac{I_p}{2U_p}}}{a^2(\tau) + s^2(\tau)},$$
(A1)

$$\cos\left(t_r - \frac{\tau}{2}\right) = \frac{-i\sqrt{\frac{I_p}{2U_p}}s(\tau) + a(\tau)\sqrt{s^2(\tau) + a^2(\tau) + \frac{I_p}{2U_p}}}{s^2(\tau) + a^2(\tau)},$$
(A2)

consider that the zero order of the return time has nothing to do with the parameter γ. We can set $\gamma = 0$ to simplify this set of relations. Then we have

$$\sin\left(t_r^{(0)} - \frac{\tau}{2}\right) = \frac{s_0(\tau)}{\sqrt{a_0^2(\tau) + s_0^2(\tau)}},$$
(A3)

$$\cos\left(t_r^{(0)} - \frac{\tau}{2}\right) = \frac{a_0(\tau)}{\sqrt{a_0^2(\tau) + s_0^2(\tau)}}.$$
(A4)

From the above equation set, it is easy to derive that

$$t_r^{(0)} = \arctan\left(\frac{s_0}{a_0}\right) + \frac{\tau_0}{2} + T\left\lfloor\left[\frac{\tau_0}{2 * 2\pi} + \frac{1}{2}\right]\right\rfloor,$$
(A5)

where the last term is added to eliminate the periodicity effect of of the arctan function. We plug the expression of a and s in Eqs. (A1) and (A2). $\tan(t_r - \tau/2)$, the division of the two, is easily obtained. Expanding $\tan(t_r - \tau/2)$ to the second order, then we have

$$t_r^{(1)} = 0,$$
(A6)

$$t_r^{(2)} = \frac{\tau_0 \cos(\tau_0) - \sin(\tau_0)}{2[\tau_0 - \sin(\tau_0)]^2}.$$
(A7)

APPENDIX B: EQUIVALENCE ZERO-ORDER RETURN ENERGY AND CLASSICAL ENERGY IN SIMPLE MAN MODEL

The zero-order return energy is

$$E_{\text{re}}^{(0)} = 8\frac{a_0^2(\tau_0)s_0^2(\tau_0)}{a_0^2(\tau_0) + s_0^2(\tau_0)}U_p.$$
(B1)

Let's multiply the numerator and the denominator $a_0^2(\tau_0) + s_0^2(\tau_0)$; the expression can be expressed in the form of $\cos(t_r - \tau_0/2)$ and $\sin(\tau_0/2)$.

$$8\frac{a_0^2(\tau_0)[a_0^2(\tau_0) + s_0^2(\tau_0)]s_0^2(\tau_0)}{[a_0^2(\tau_0) + s_0^2(\tau_0)]^2}U_p$$

$$= 2U_p\left[2\cos\left(t_r - \frac{\tau_0}{2}\right)\sin\left(\frac{\tau_0}{2}\right)\right]^2$$

$$= 2U_p[\sin(t_r) - \sin(t_r - \tau_0)]^2$$

$$= E_c.$$
(B2)

APPENDIX C: DERIVATION OF FIRST-ORDER CANONICAL MOMENTUM

We plug τ and t_r in p_{st} and expand the expression to second order, then the first-order canonical momentum takes the form

$$p_{\text{st}}^{(1)} = -\frac{\tau_1}{\tau_0^2}\left[\cos\left(t_r^{(0)}\right) - \cos\left(t_r^{(0)} - \tau_0\right) + \tau_0\sin\left(t_r^{(0)} - \tau_0\right)\right].$$
(C1)

We dismantle the function of $t_r^{(0)}$ and $t_r^{(0)} - \tau_0$ into the form of $t_r^{(0)} - \tau_0/2$ and $\tau_0/2$, then the expression can be expressed as

$$p_{\text{st}}^{(1)} = -2\sin\left(\frac{\tau_0}{2}\right)\sin\left(t_r^{(0)} - \frac{\tau_0}{2}\right)$$

$$+ \tau_0\left(\cos\left(\frac{\tau_0}{2}\right)\sin\left(t_r^{(0)} - \frac{\tau_0}{2}\right)\right.$$

$$\left. - \sin\left(\frac{\tau_0}{2}\right)\cos\left(t_r^{(0)} - \frac{\tau_0}{2}\right)\right)$$

$$= -\frac{2s_0^2}{\sqrt{a_0^2 + s_0^2}} + \tau_0\left[\frac{s_0}{\sqrt{a_0^2 + s_0^2}}\left(a_0 + \frac{2s_0}{\tau_0}\right)\right.$$

$$\left. - \frac{a_0 s_0}{\sqrt{a_0^2 + s_0^2}}\right]$$

$$= 0.$$

[1] C. Hofmann, A. Bray, W. Koch, H. Ni, and N. I. Shvetsov-Shilovski, Quantum battles in attoscience: Tunnelling, Eur. Phys. J. D **75**, 208 (2021).

[2] A. S. Landsman and U. Keller, Attosecond science and the tunnelling time problem, Phys. Rep. **547**, 1 (2015).

[3] A. S. Landsman, M. Weger, J. Maurer, R. Boge, A. Ludwig, S. Heuser, C. Cirelli, L. Gallmann, and U. Keller, Ultrafast resolution of tunneling delay time, Optica **1**, 343 (2014).

[4] U. S. Sainadh, H. Xu, X. Wang, A. Atia-Tul-Noor, W. C. Wallace, N. Douguet, A. Bray, I. Ivanov, K. Bartschat, A. Kheifets, R. T. Sang, and I. V. Litvinyuk, Attosecond angular streaking and tunnelling time in atomic hydrogen, Nature (London) **568**, 75 (2019).

[5] D. Shafir, H. Soifer, B. D. Bruner, M. Dagan, Y. Mairesse, S. Patchkovskii, M. Y. Ivanov, O. Smirnova, and N. Dudovich, Resolving the time when an electron exits a tunnelling barrier, Nature (London) **485**, 343 (2012).

[6] L. Torlina and O. Smirnova, Coulomb time delays in high harmonic generation, New J. Phys. **19**, 023012 (2017).

[7] M. F. Ciappina, J. A. Pérez-Hernández, A. S. Landsman, T. Zimmermann, M. Lewenstein, L. Roso, and F. Krausz, Carrier-Wave Rabi-Flopping Signatures in High-Order Harmonic Generation for Alkali Atoms, Phys. Rev. Lett. **114**, 143902 (2015).

[8] L. Ortmann, J. A. Perez-Hernandez, M. F. Ciappina, J. Schotz, A. Chacon, G. Zeraouli, M. F. Kling, L. Roso, M. Lewenstein, and A. S. Landsman, Emergence of a Higher Energy Structure in Strong Field Ionization with Inhomogeneous Electric Fields, Phys. Rev. Lett. **119**, 053204 (2017).

[9] L. Ortmann and A. S. Landsman, Analysis of the higher-energy structure in strong-field ionization with inhomogeneous electric fields, Phys. Rev. A **97**, 023420 (2018).

[10] X.-Z. Gao, A. S. Landsman, H. Wang, P. Huang, Y. Zhang, B. Wang, Y. Wang, H. Cao, Y. Fu, and L.-W. Pi, Analysis of a higher-energy structure in nanotip enhanced fields, New J. Phys. **23**, 113017 (2021).

[11] H. Ni, U. Saalmann, and J.-M. Rost, Tunneling Ionization Time Resolved By Backpropagation, Phys. Rev. Lett. **117**, 023002 (2016).

[12] H. Ni, N. Eicke, C. Ruiz, J. Cai, F. Oppermann, N. I. Shvetsov-Shilovski, and L.-W. Pi, Tunneling criteria and a nonadiabatic term for strong-field ionization, Phys. Rev. A **98**, 013411 (2018).

[13] H. Ni, U. Saalmann, and J.-M. Rost, Tunneling exit characteristics from classical backpropagation of an ionized electron wave packet, Phys. Rev. A **97**, 013426 (2018).

[14] A. N. Pfeiffer, C. Cirelli, A. S. Landsman, M. Smolarski, D. Dimitrovski, L. B. Madsen, and U. Keller, Probing the Longitudinal Momentum Spread of the Electron Wave Packet at the Tunnel Exit, Phys. Rev. Lett. **109**, 083002 (2012).

[15] M. Han, P. Ge, Y. Fang, X. Yu, Z. Guo, X. Ma, Y. Deng, Q. Gong, and Y. Liu, Unifying Tunneling Pictures of Strong-Field Ionization with an Improved Attoclock, Phys. Rev. Lett. **123**, 073201 (2019).

[16] L.-W. Pi and A. Landsman, Attosecond time delay in photoionization of noble-gas and halogen atoms, Appl. Sci. **8**, 322 (2018).

[17] J. Li, J. Lu, A. Chew, S. Han, J. Li, Y. Wu, H. Wang, S. Ghimire, and Z. Chang, Attosecond science based on high harmonic generation from gases and solids, Nat. Commun. **11**, 2748 (2020).

[18] X. Ren, J. Li, Y. Yin, K. Zhao, A. Chew, Y. Wang, S. Hu, Y. Cheng, E. Cunningham, Y. Wu, M. Chini, and Z. Chang, Attosecond light sources in the water window, J. Opt. **20**, 023001 (2018).

[19] F. Calegari, G. Sansone, S. Stagira, C. Vozzi, and M. Nisoli, Advances in attosecond science, J. Phys. B: At., Mol. Opt. Phys. **49**, 062001 (2016).

[20] P. B. Corkum, Plasma Perspective on Strong Field Multiphoton Ionization, Phys. Rev. Lett. **71**, 1994 (1993).

[21] K. J. Schafer, B. Yang, L. F. DiMauro, and K. C. Kulander, Above Threshold Ionization Beyond the High Harmonic Cutoff, Phys. Rev. Lett. **70**, 1599 (1993).

[22] R. L. Sandberg, C. Song, P. W. Wachulak, D. A. Raymondson, A. Paul, B. Amirbekian, E. Lee, A. E. Sakdinawat, C. La-O-Vorakiat, M. C. Marconi, C. S. Menoni, M. M. Murnane, J. J. Rocca, H. C. Kapteyn, and J. Miao, High numerical aperture

tabletop soft x-ray diffraction microscopy with 70-nm resolution, Proc. Natl. Acad. Sci. **105**, 24 (2008).

[23] A. Ravasio, D. Gauthier, F. R. N. C. Maia, M. Billon, J.-P. Caumes, D. Garzella, M. Géléoc, O. Gobert, J.-F. Hergott, A.-M. Pena, H. Perez, B. Carré, E. Bourhis, J. Gierak, A. Madouri, D. Mailly, B. Schiedt, M. Fajardo, J. Gautier, P. Zeitoun, P. H. Bucksbaum, J. Hajdu, and H. Merdji, Single-Shot Diffractive Imaging with a Table-Top Femtosecond Soft X-Ray Laser-Harmonics Source, Phys. Rev. Lett. **103**, 028104 (2009).

[24] M. Lewenstein, P. Balcou, M. Y. Ivanov, A. L'Huillier, and P. B. Corkum, Theory of high-harmonic generation by low-frequency laser fields, Phys. Rev. A **49**, 2117 (1994).

[25] M. Ivanov, Ionization in strong low-frequency fields, in *Attosecond and XUV Physics: Ultrafast Dynamics and Spectroscopy*, edited by T. Schultz and M. Vrakking (Wiley-VCH, Weinham, Germany, 2014), pp. 179–200.

[26] A.-T. Le, H. Wei, C. Jin, and C. D. Lin, Strong-field approximation and its extension for high-order harmonic generation with mid-infrared lasers, J. Phys. B: At. Mol. Opt. Phys. **49**, 053001 (2016).

[27] K. Amini, J. Biegert, F. Calegari, A. Chacón, M. F. Ciappina, A. Dauphin, D. K. Efimov, C. Figueira de Morisson Faria, K. Giergiel, P. Gniewek, A. S. Landsman, M. Lesiuk, M. Mandrysz, A. S. Maxwell, R. Moszyński, L. Ortmann, J. Antonio Pérez-Hernández, A. Picón, E. Pisanty, J. Prauzner-Bechcicki, K. Sacha, N. Suárez, A. Zaïr, J. Zakrzewski, and M. Lewenstein, Symphony on strong field approximation, Rep. Prog. Phys. **82**, 116001 (2019).

[28] B. Wang, X. Li, and P. Fu, Polarization effects in high-harmonic generation in the presence of static-electric field, Phys. Rev. A **59**, 2894 (1999).

[29] D. B. Milošević and B. Piraux, High-order harmonic generation in a bichromatic elliptically polarized laser field, Phys. Rev. A **54**, 1522 (1996).

[30] P. Antoine, A. L'Huillier, M. Lewenstein, P. Salières, and B. Carré, Theory of high-order harmonic generation by an elliptically polarized laser field, Phys. Rev. A **53**, 1725 (1996).

[31] D. B. Milosevic, Cut-off law for high-harmonic generation by an elliptically polarized laser field, J. Phys. B: At. Mol. Opt. Phys. **33**, 2479 (2000).

[32] E. Neyra, F. Videla, M. F. Ciappina, J. A. Pérez-Hernández, L. Roso, M. Lewenstein, and G. A. Torchia, High-order harmonic generation driven by inhomogeneous plasmonics fields spatially bounded: Influence on the cut-off law, J. Opt. **20**, 034002 (2018).

[33] P. Ye, X. He, H. Teng, M. Zhan, S. Zhong, W. Zhang, L. Wang, and Z. Wei, Full Quantum Trajectories Resolved High-Order Harmonic Generation, Phys. Rev. Lett. **113**, 073601 (2014).

[34] D. B. Milošević, Quantum-orbit analysis of high-order harmonic generation by bicircular field, J. Mod. Opt. **66**, 47 (2019).

[35] E. Pisanty, M. F. Ciappina, and M. Lewenstein, The imaginary part of the high-harmonic cutoff, J. Phys. Photonics **2**, 034013 (2020).

[36] M. Lewenstein, P. Salières, and A. L'Huillier, Phase of the atomic polarization in high-order harmonic generation, Phys. Rev. A **52**, 4747 (1995).

[37] G. G. Brown, D. H. Ko, C. Zhang, and P. B. Corkum, Attosecond measurement via high-order harmonic generation in low-frequency fields, Phys. Rev. A **105**, 023520 (2022).

[38] Y. Chen, Dynamic of rescattering-electron wave packets in strong and short-wavelength laser fields: Roles of coulomb potential and excited states, Phys. Rev. A **84**, 043423 (2011).

[39] Y. Chen and B. Zhang, Role of excited states in the emission times of harmonics from asymmetric molecules, Phys. Rev. A **86**, 023415 (2012).

[40] C. J. Joachain, N. J. Kylstra, and R. M. Potvliege, *Atoms in Intense Laser Fields* (Cambridge University Press, Cambridge, England, 2011), p. 315.

[41] D. B. Milošević and W. Becker, Role of long quantum orbits in high-order harmonic generation, Phys. Rev. A **66**, 063417 (2002).